

**Probing and evaluating anion- $\pi$  interaction in *meso*-dinitrophenyl functionalized calix[4]pyrrole isomers**

Ajeong Kim,<sup>a</sup> Rashid Ali,<sup>a</sup> Seok Ho Park,<sup>b</sup> Yong-Hoon Kim <sup>\*b</sup> and Jung Su Park <sup>\*a</sup>

[a] Department of Chemistry, Sookmyung Woman's University, Seoul 140-742, Korea

[b] National Academy of Agricultural Science, Rural Development Administration, Department of Agricultural Engineering, 310 Nongsangmyeng-ro, Wansan-gu, Jeonju, Korea

**Contents**

- I. X-ray crystallographic analyses.
- II. 1. Continuous variation plots (Job plots).  
2. Absorbance spectra and their binding isotherms analyses.  
3. <sup>1</sup>H NMR studies.

## I. X-ray Crystallographic Analyses.

All structures were solved by direct methods and refined by full-matrix least-squares on  $F^2$  with anisotropic displacement parameters for the non-H atoms using SHELXL-97. The function,  $\Sigma w(|Fo|^2 - |Fc|^2)^2$ , was minimized, where  $w = 1/[(|Fo|)^2 + (X^*P)^2 + (Y^*P)]$  and  $P = (|Fo|^2 + 2|Fc|^2)/3$  and the parameters, X and Y, are suggested during the refinement process. The hydrogen atoms were calculated in ideal positions with isotropic displacement parameters set to 1.2xUeq of the attached atom (1.5xUeq for methyl hydrogen atoms). Neutral atom scattering factors and values used to calculate the linear absorption coefficient are from the International Tables for X-ray Crystallography (1992) (*sI*). All the calculations were carried out with the SHELXTL program. The details of the crystallographic data for the complexes **1** containing TBAF, TBACl, TBABr, TBAI, TBANO<sub>3</sub>, TBAOAc, TEAHCO<sub>3</sub>, TBAHSO<sub>4</sub>, TBAH<sub>2</sub>PO<sub>4</sub> are summarized in Table S1. Further details of the individual structures can be obtained from the Cambridge Crystallographic Data Centre by quoting CCDC 1482084-1482092.

**Table S1.** Selected crystal data and refinement parameters

	<b>1-TBAF/Cl</b>	<b>1-TBACl</b>	<b>1-TBABr</b>
Empirical formula	C <sub>54</sub> H <sub>72</sub> Cl <sub>0.63</sub> F <sub>0.37</sub> N <sub>9</sub> O <sub>8</sub>	C <sub>54</sub> H <sub>72</sub> ClN <sub>9</sub> O <sub>8</sub>	C <sub>54</sub> H <sub>72</sub> BrN <sub>9</sub> O <sub>8</sub>
Crystal system	Monoclinic	Monoclinic	Monoclinic
Space group	P2 <sub>1</sub> n	P2 <sub>1</sub> n	P2 <sub>1</sub> n
Crystal color	Orange	Orange	Orange
a (Å)	12.9168(7)	13.0109(16)	12.865(3)
b (Å)	18.9009(10)	18.833(2)	18.623(5)
c (Å)	22.5896(12)	22.702(3)	22.483(6)
α (deg)	90	90	90
β (deg)	90.650(3)	90.423(3)	90.143(4)
γ (deg)	90	90	90
Volume (Å <sup>3</sup> )	5514.7(5)	5562.6(12)	5387(2)
Z	4	4	4
θ range	1.40 to 27.50	3.10 to 27.48	1.42 to 25.00
Completeness to θ	99.7	98.4	95.7 %
Absorption correction	Semi-empirical	Semi-empirical	Semi-empirical
Data/restraints/parameters	12621 / 0 / 668	12550 / 0 / 659	9070 / 0 / 659
Goodness-of-fit on F <sup>2</sup>	1.278	1.099	1.366
Final R indices [I>2δ(I)]	R <sub>1</sub> = 0.0757 wR <sub>2</sub> = 0.1577	R <sub>1</sub> = 0.0666 wR <sub>2</sub> = 0.1447	R <sub>1</sub> = 0.1197 wR <sub>2</sub> = 0.2515
R indices (all data)	R <sub>1</sub> = 0.1487 wR <sub>2</sub> = 0.2084	R <sub>1</sub> = 0.1187 wR <sub>2</sub> = 0.1677	R <sub>1</sub> = 0.1348 wR <sub>2</sub> = 0.2598
CCDC number	<b>CCDC 1482087</b>	<b>CCDC 1482085</b>	<b>CCDC 1482084</b>

	<b>1-TBAI</b>	<b>1-TBANO<sub>3</sub></b>	<b>1-TBAAcO</b>
Empirical formula	C <sub>54</sub> H <sub>72</sub> IN <sub>9</sub> O <sub>8</sub>	C <sub>54</sub> H <sub>72</sub> N <sub>10</sub> O <sub>11</sub>	C <sub>56</sub> H <sub>75</sub> N <sub>9</sub> O <sub>10</sub>
Crystal system	Orthorhombic	Monoclinic	Monoclinic
Space group	Pca21	P2 <sub>1</sub> n	P2 <sub>1</sub> n
Crystal color	Orange	Orange	Orange
a (Å)	21.335(12)	12.8705(12)	12.773(4)
b (Å)	15.168(8)	18.6776(18)	19.067(6)
c (Å)	37.948(19)	23.141(2)	23.221(7)
α (deg)	90	90	90
β (deg)	90	90.418(2)	91.690(4)
γ (deg)	90	90	90
Volume (Å <sup>3</sup> )	12280	5562.7(9)	5653(3)
Z	8	4	4
θ range	1.34 to 25.00	3.07 to 27.49	1.38 to 25.00
Completeness to θ	95.4	99.0	99.9
Absorption correction	Semi-empirical	Semi-empirical	Semi-empirical
Data/restraints/parameters	16640 / 133 / 1309	12637 / 0 / 686	9943 / 0 / 687
Goodness-of-fit on F <sup>2</sup>	1.016	1.057	1.196
Final R indices [I>2δ(I)]	R <sub>1</sub> = 0.0688 wR <sub>2</sub> = 0.1835	R <sub>1</sub> = 0.0688 wR <sub>2</sub> = 0.1394	R <sub>1</sub> = 0.0636 wR <sub>2</sub> = 0.1269
R indices (all data)	R <sub>1</sub> = 0.0916 wR <sub>2</sub> = 0.2090	R <sub>1</sub> = 0.1598 wR <sub>2</sub> = 0.1714	R <sub>1</sub> = 0.0968 wR <sub>2</sub> = 0.1492
CCDC number	<b>CCDC 1482086</b>	<b>CCDC 1482091</b>	<b>CCDC 1482092</b>

	<b>1-TEAHCO3</b>	<b>1-TBAHSO4</b>	<b>1-TBAH2PO4</b>
Empirical formula	C <sub>58</sub> H <sub>60</sub> C <sub>16</sub> N <sub>10</sub> O <sub>14</sub>	C <sub>70</sub> H <sub>110</sub> N <sub>10</sub> O <sub>16</sub> S <sub>2</sub>	C <sub>72</sub> H <sub>116</sub> Cl <sub>3</sub> N <sub>10</sub> O <sub>18</sub> P <sub>2</sub>
Crystal system	Triclinic	Monoclinic	Triclinic
Space group	P-1	P2 <sub>1</sub> n	P-1
Crystal color	Orange	Orange	Orange
a (Å)	11.224(6)	14.239(3)	18.5581(12)
b (Å)	13.636(8)	21.245(4)	19.3272(12)
c (Å)	22.374(13)	24.510(5)	23.1017(15)
α (deg)	101.011(8)	90	86.218(2)
β (deg)	98.751(9)	92.19(3)	87.845(2)
γ (deg)	91.381(11)	90	81.721(2)
Volume (Å <sup>3</sup> )	3317(3)	7409(3)	8178.5(9)
Z	2	4	2
θ range	2.32 to 25.00	3.02 to 25.00	3.04 to 25.00
Completeness to θ	97.8	95.3	96.5 %
Absorption correction	Semi-empirical	Semi-empirical	Semi-empirical
Data/restraints/parameters	11463 / 19 / 842	12438 / 0 / 897	27777 / 24 / 1923
Goodness-of-fit on F <sup>2</sup>	1.354	1.033	1.045
Final R indices [I>2δ(I)]	R <sub>1</sub> = 0.1123 wR <sub>2</sub> = 0.2536	R <sub>1</sub> = 0.0504 wR <sub>2</sub> = 0.1155	R <sub>1</sub> = 0.0686 wR <sub>2</sub> = 0.1846
R indices (all data)	R <sub>1</sub> = 0.1301 wR <sub>2</sub> = 0.2644	R <sub>1</sub> = 0.0798 wR <sub>2</sub> = 0.1292	R <sub>1</sub> = 0.0900 wR <sub>2</sub> = 0.2032
CCDC number	<b>CCDC 1482089</b>	<b>CCDC 1482090</b>	<b>CCDC 1482088</b>

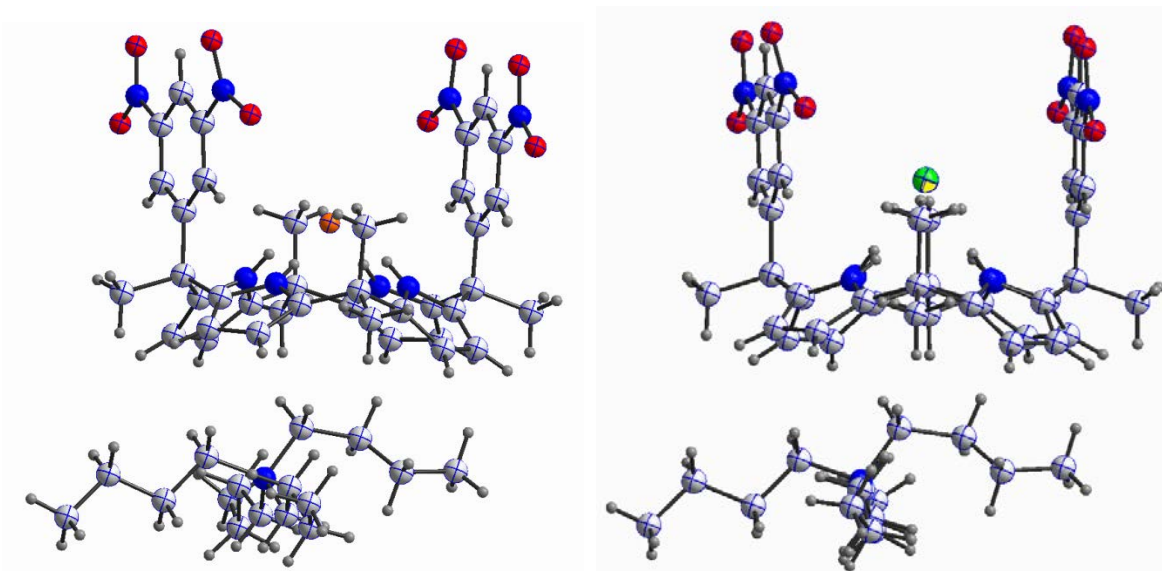


**Figure S1.** X-ray crystal structure of **1**·TBAF (left, partially occupied chloride was omitted for the clarity) and **1**·TBACl (right).

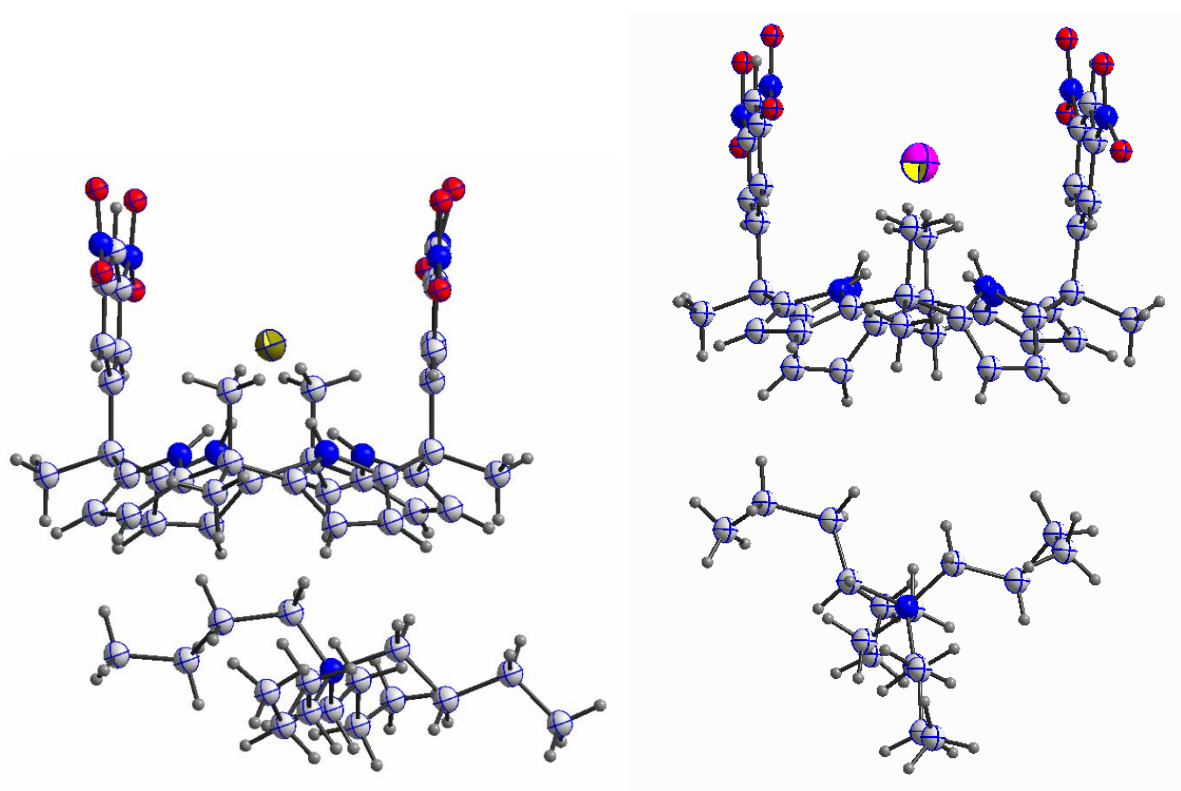


**Figure S2.** X-ray crystal structures of  $\mathbf{1} \odot \text{TBABr}$  (left) and  $\mathbf{1} \odot \text{TBAI}$  (right).

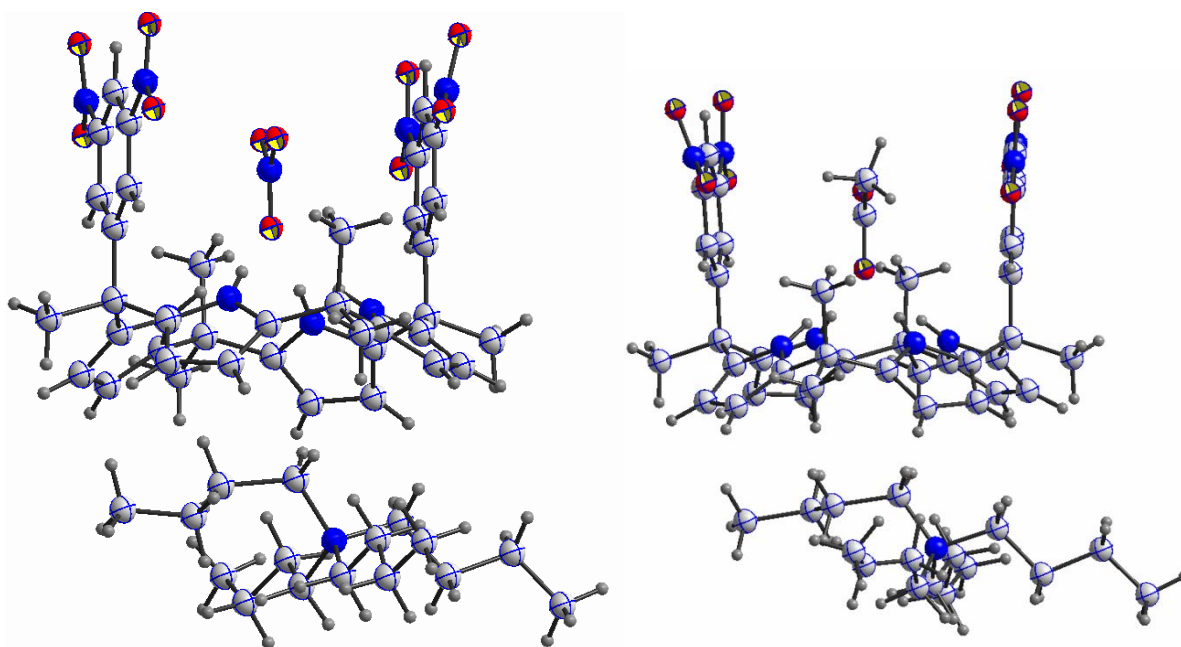


**Figure S3.** X-ray crystal structures of  $\mathbf{1} \odot \text{TBANO}_3$  (left) and  $\mathbf{1} \odot \text{TBAAcO}$  .

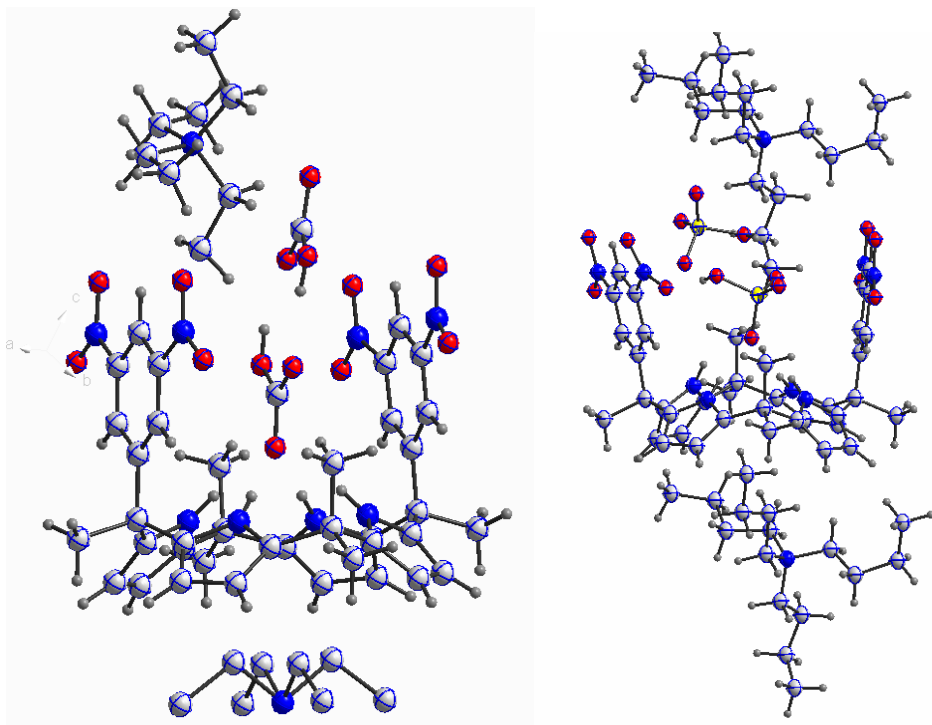


**Figure S4.** X-ray crystal structures of  $\mathbf{1} \square \text{TEA}(\text{HCO}_3)_2$  (left) and  $\mathbf{1} \square (\text{TBAHSO}_4)_2$  (right).

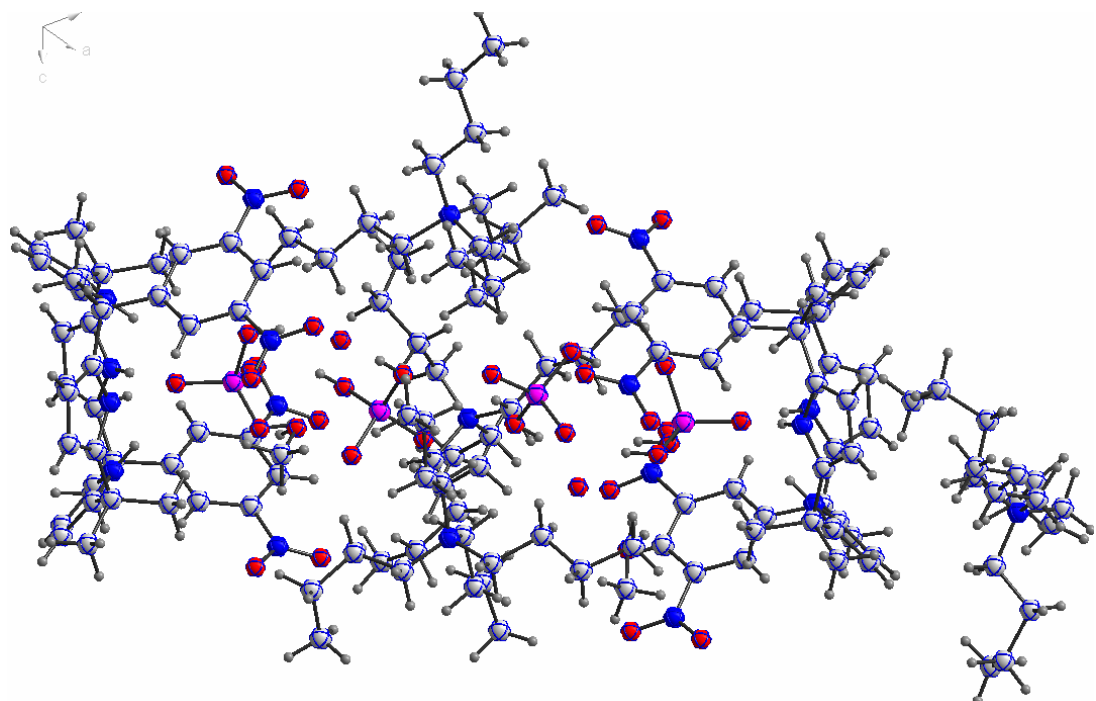


**Figure S5.** X-ray crystal structures of  $\mathbf{1}_2 \square (\text{TBAH}_2\text{PO}_4)_4$ .

## II-1. Continuous variation plots (Job plots)

Continuous variation plots well-known as Job plots are used to determine the stoichiometry of binding events. In this method, the total molar concentration of two monomers units are held constant, but their mole fractions are varied. In the present study, Job plots of **1** and **2** with these anions were constructed at invariant total concentration of 0.2 mM in acetonitrile solution at ambient temperature. As can be seen by the inspection of Figures 1 and 2, the maximum at a mole fraction,  $x$ , 0.5 was observed for all the anions. This value is as expected for a 1:1 binding between host DNP-C4Ps and a variety of guest anions.

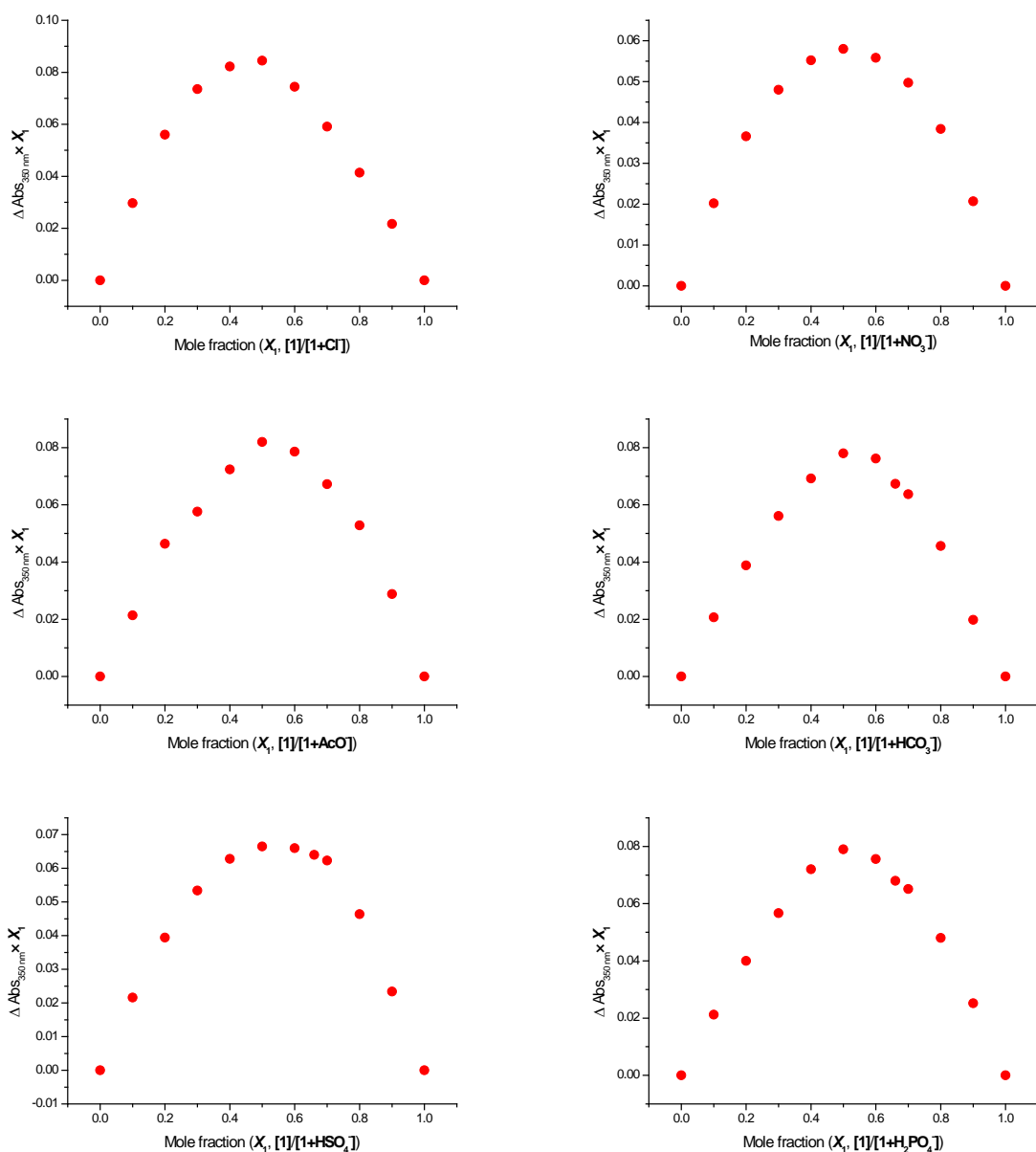


**Figure S6.** Job plots for DNP-C4P *cis*-**1** + anions, recorded in acetonitrile solution at ambient temperature. These plots were constructed by plotting the product of the change in the absorption at 350 nm and the mole-fraction of **1** vs. the mole fraction of DNP-C4P *cis*-**1**.

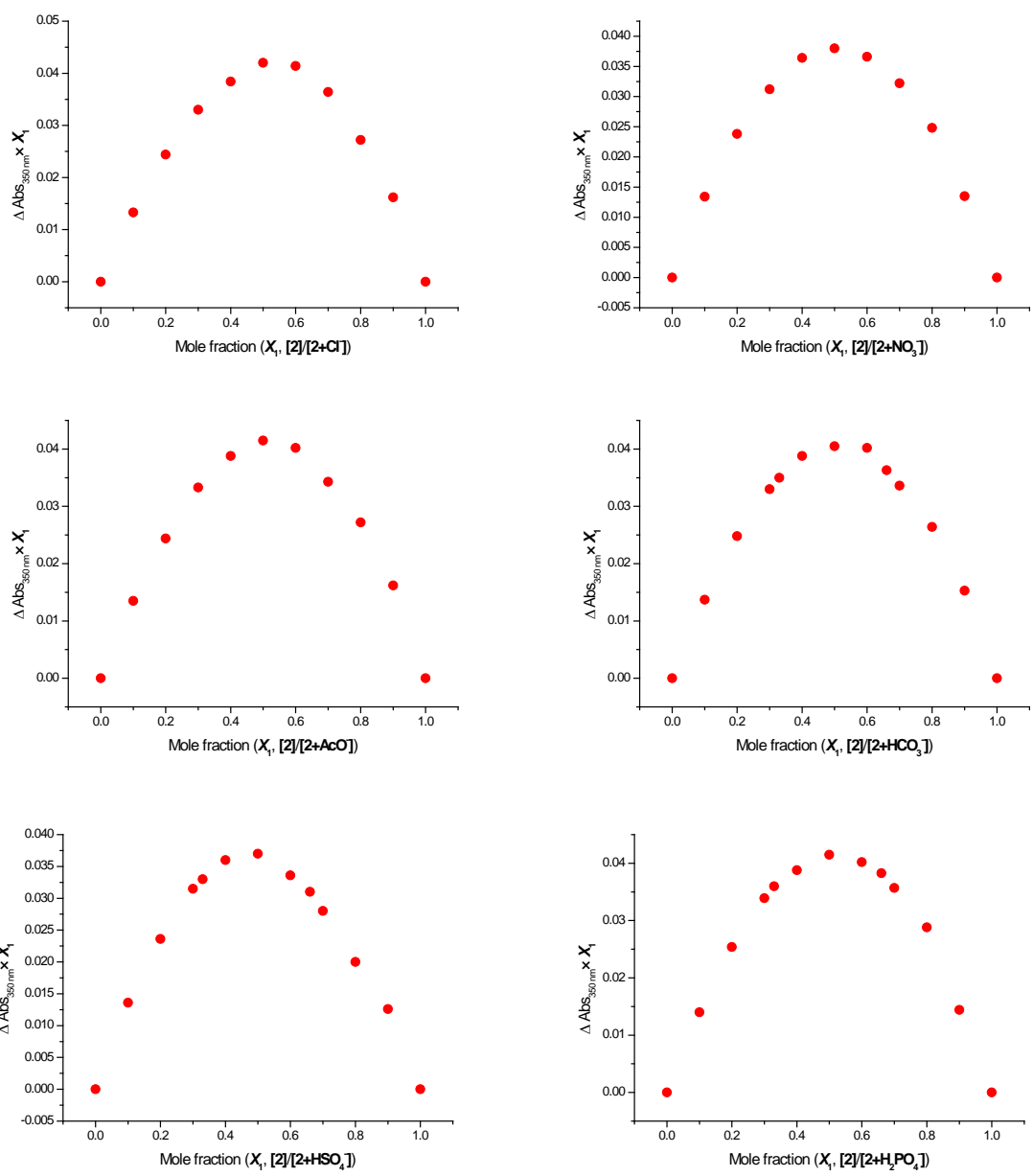


**Figure S7.** Job plots for DNP-C4P *trans*-2 + anions, recorded in acetonitrile solution at ambient temperature. These plots were constructed by plotting the product of the change in the absorption at 350 nm and the mole-fraction of **2** vs. the mole fraction of DNP-C4P *trans*-2.

## I-2. Binding isotherms analyses of DNP-C4P with diverse anions.

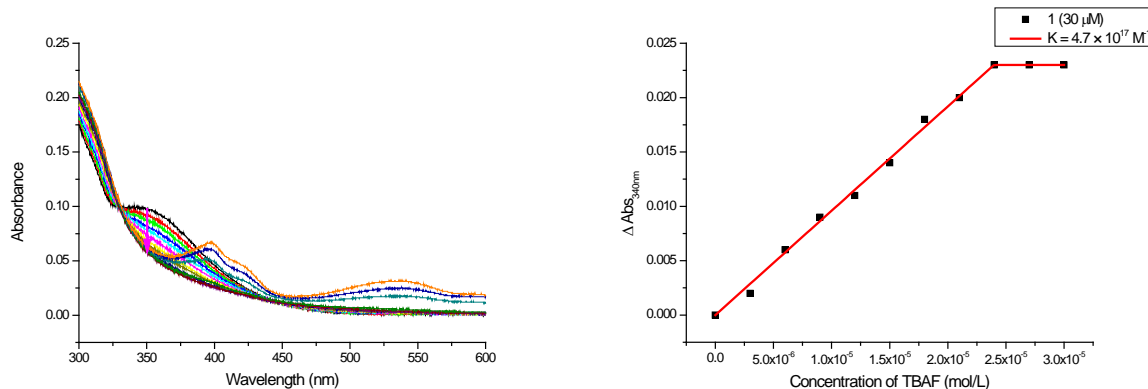


**Figure S8.** Changes in the electronic spectrum of DNP-C4P *cis*-1 (acetonitrile solution; ambient temperature) seen upon the progressive addition of TBAF (left) and the corresponding binding isotherm analysis (right).

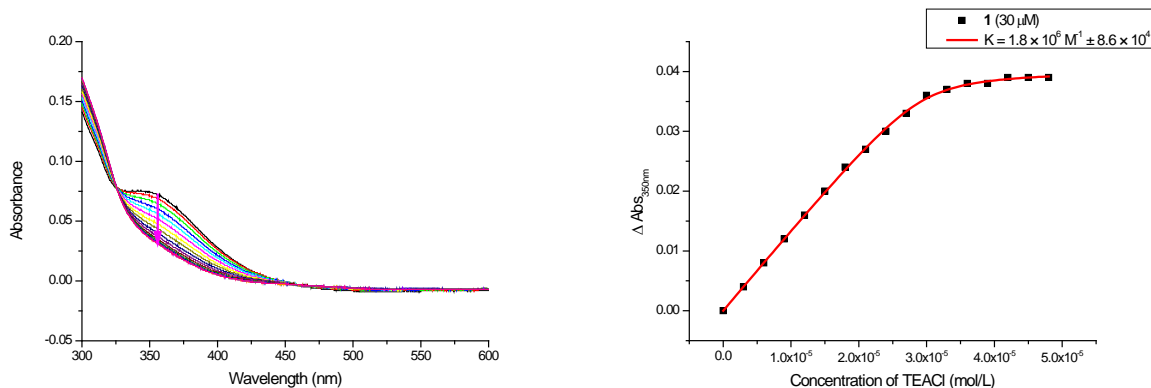


**Figure S9.** Changes in the electronic spectrum of DNP-C4P *cis*-1 (acetonitrile solution; ambient temperature) seen upon the progressive addition of TEACl (left) and the corresponding binding isotherm analysis (right).

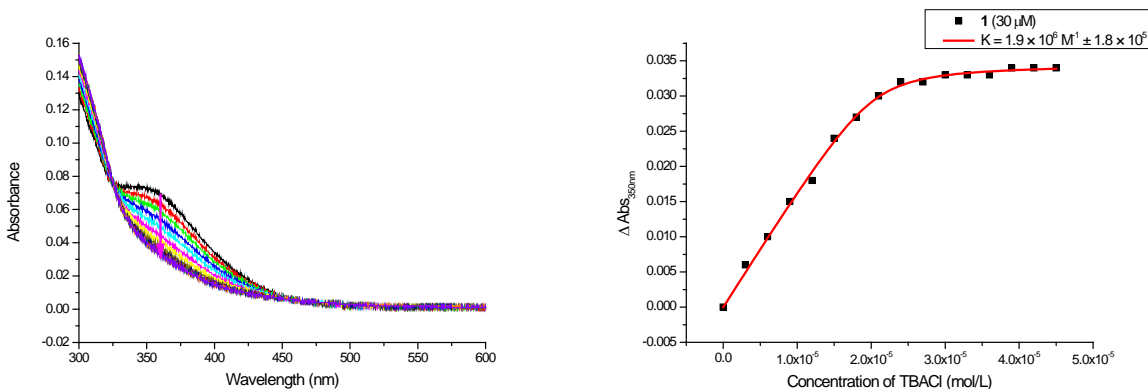


**Figure S10.** Changes in the electronic spectrum of DNP-C4P *cis*-1 (acetonitrile solution; ambient temperature) seen upon the progressive addition of TBACl (left) and the corresponding binding isotherm analysis (right).

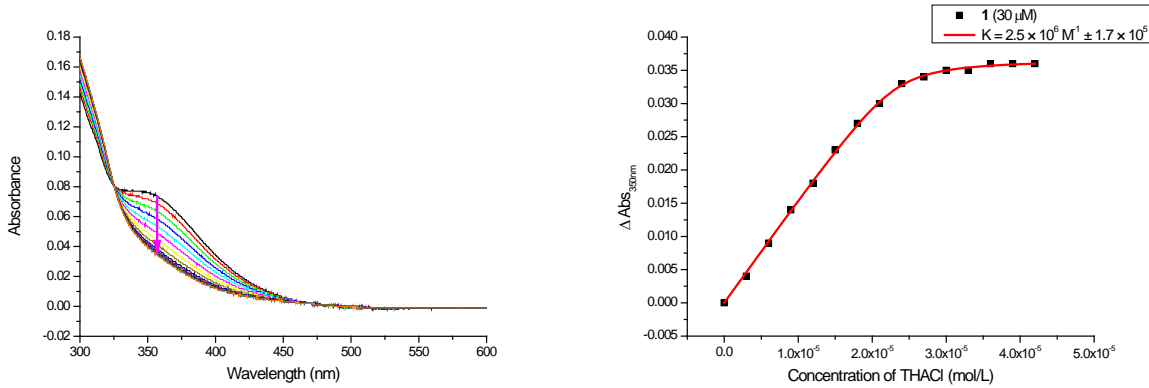


**Figure S11.** Changes in the electronic spectrum of DNP-C4P *cis*-**1** (acetonitrile solution; ambient temperature) seen upon the progressive addition of THACl (left) and the corresponding binding isotherm analysis (right).

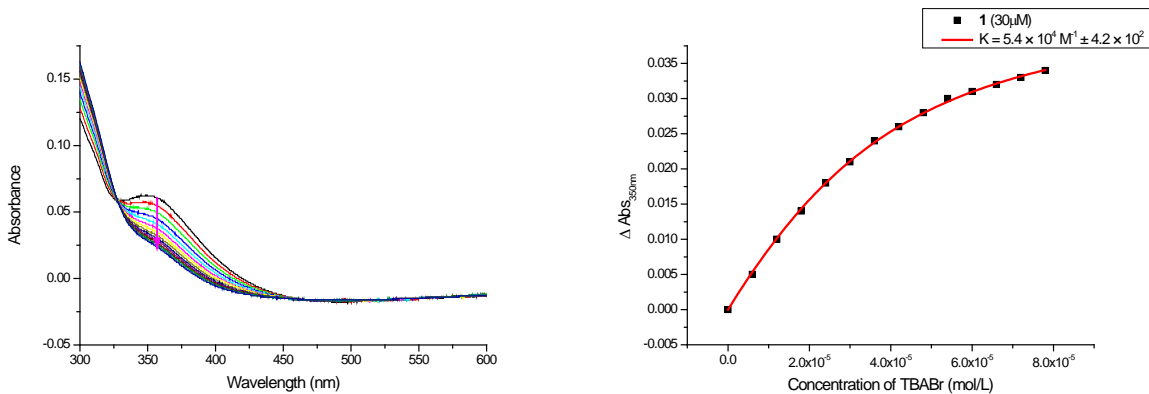


**Figure S12.** Changes in the electronic spectrum of DNP-C4P *cis*-**1** (acetonitrile solution; ambient temperature) seen upon the progressive addition of TBABr (left) and the corresponding binding isotherm analysis (right).

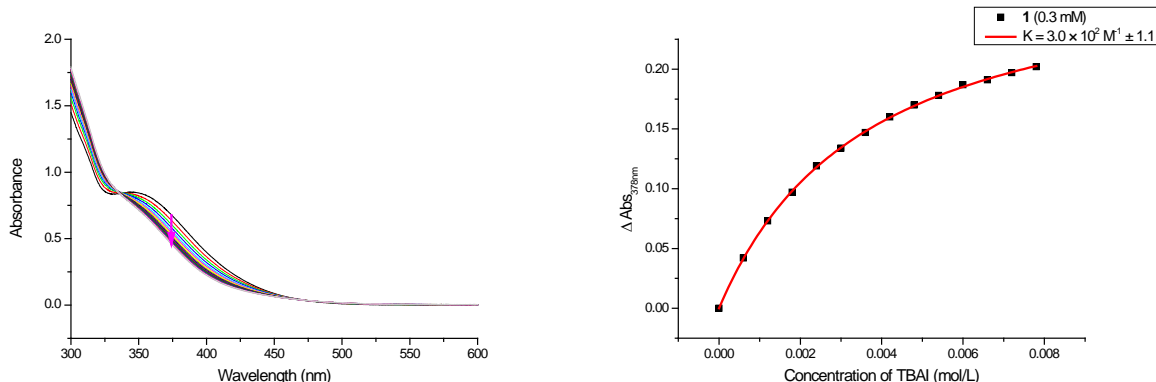


**Figure S13.** Changes in the electronic spectrum of DNP-C4P *cis*-**1** (acetonitrile solution; ambient temperature) seen upon the progressive addition of TBAI (left) and the corresponding binding isotherm analysis (right).

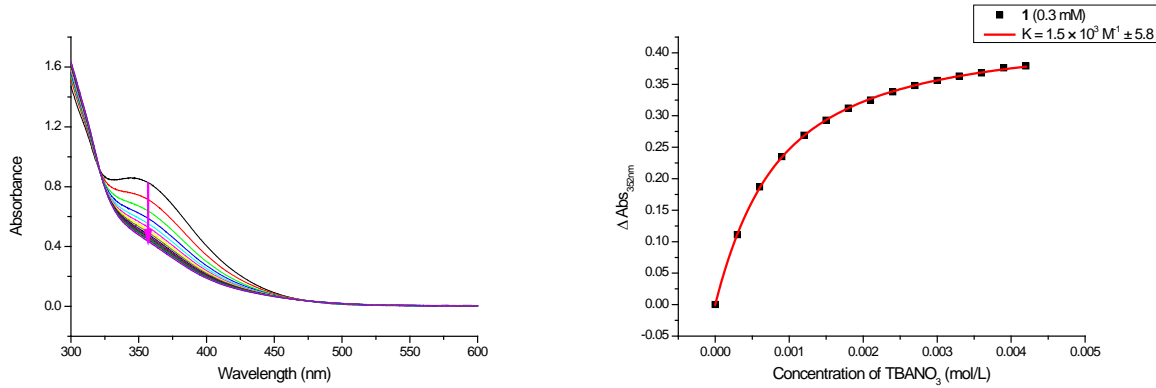


**Figure S14.** Changes in the electronic spectrum of DNP-C4P *cis*-1 (acetonitrile solution; ambient temperature) seen upon the progressive addition of TBANO<sub>3</sub> (left) and the corresponding binding isotherm analysis (right).

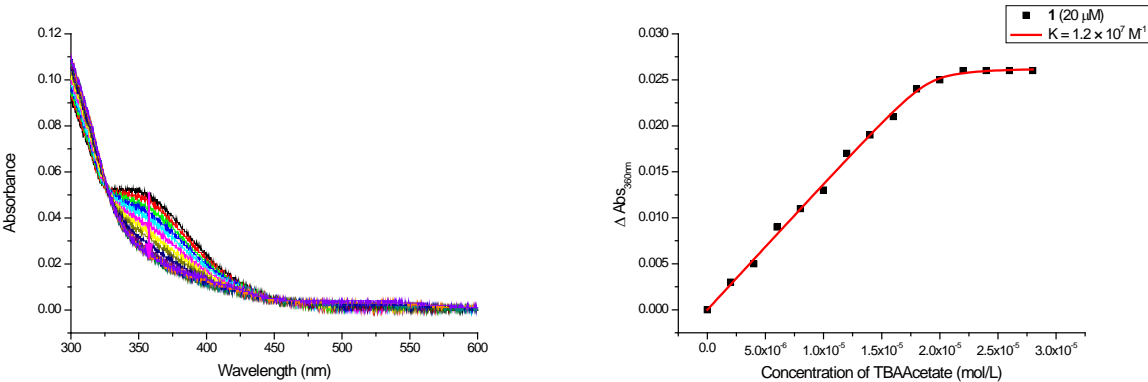


**Figure S15.** Changes in the electronic spectrum of DNP-C4P *cis*-1 (acetonitrile solution; ambient temperature) seen upon the progressive addition of TBAAcetate (left) and the corresponding binding isotherm analysis (right).

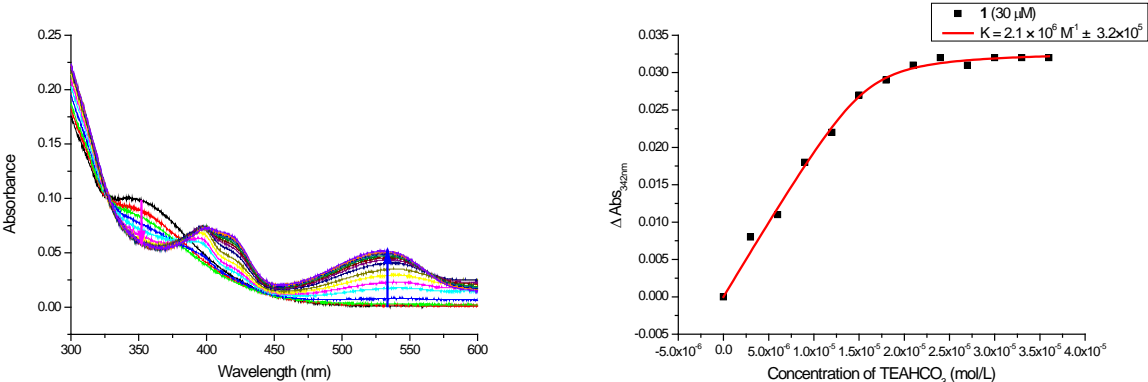


**Figure S16.** Changes in the electronic spectrum of DNP-C4P *cis*-1 (acetonitrile solution; ambient temperature) seen upon the progressive addition of TEAHCO<sub>3</sub> (left) and the corresponding binding isotherm analysis (right).

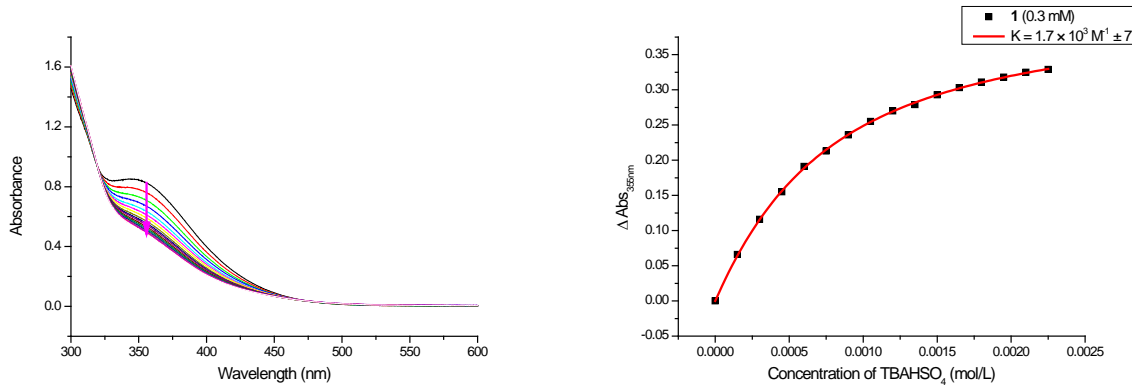


**Figure S17.** Changes in the electronic spectrum of DNP-C4P *cis*-**1** (acetonitrile solution; ambient temperature) seen upon the progressive addition of TBAHSO<sub>4</sub> (left) and the corresponding binding isotherm analysis (right).

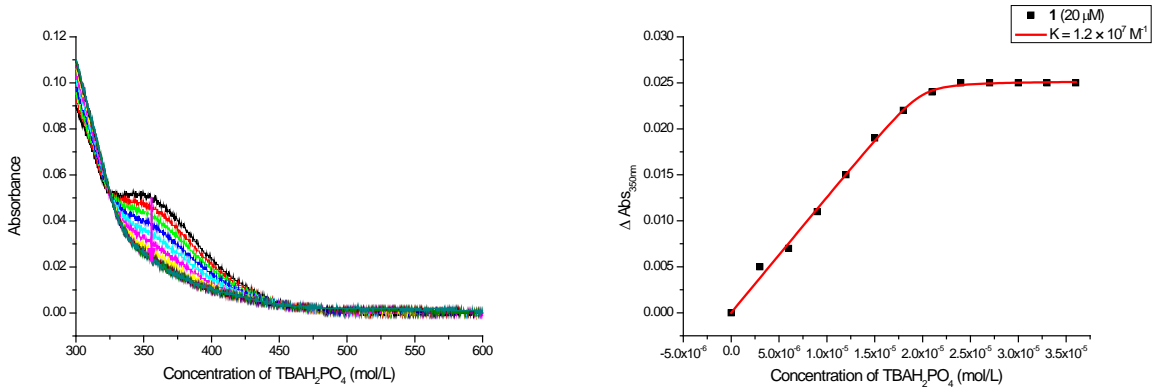


**Figure S18.** Changes in the electronic spectrum of DNP-C4P *cis*-**1** (acetonitrile solution; ambient temperature) seen upon the progressive addition of TBAH<sub>2</sub>PO<sub>4</sub> (left) and the corresponding binding isotherm analysis (right).

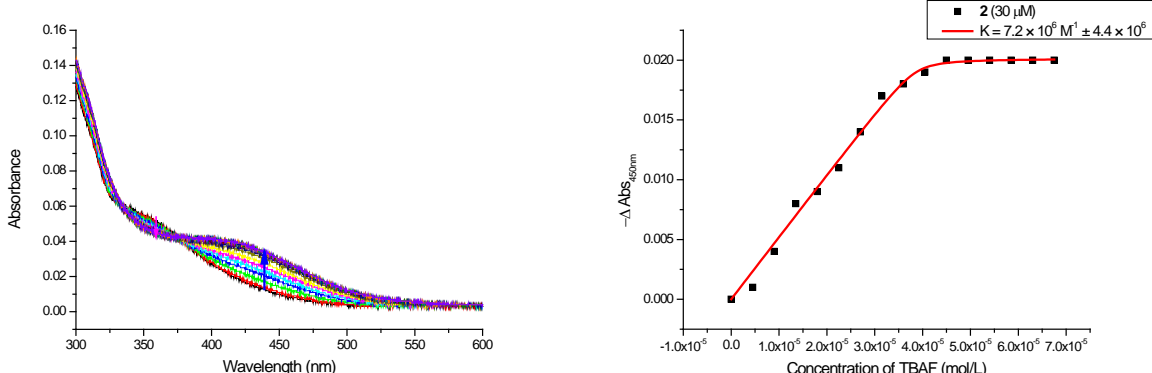


**Figure S19.** Changes in the electronic spectrum of DNP-C4P *trans*-**2** (acetonitrile solution; ambient temperature) seen upon the progressive addition of TBAF (left) and the corresponding binding isotherm analysis (right).

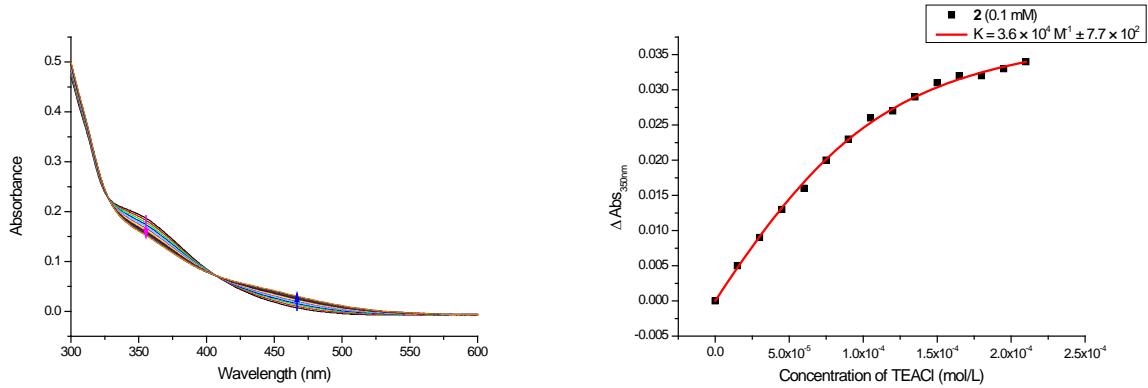


**Figure S20.** Changes in the electronic spectrum of DNP-C4P *trans*-**2** (acetonitrile solution; ambient temperature) seen upon the progressive addition of TEACl (left) and the corresponding binding isotherm analysis (right).

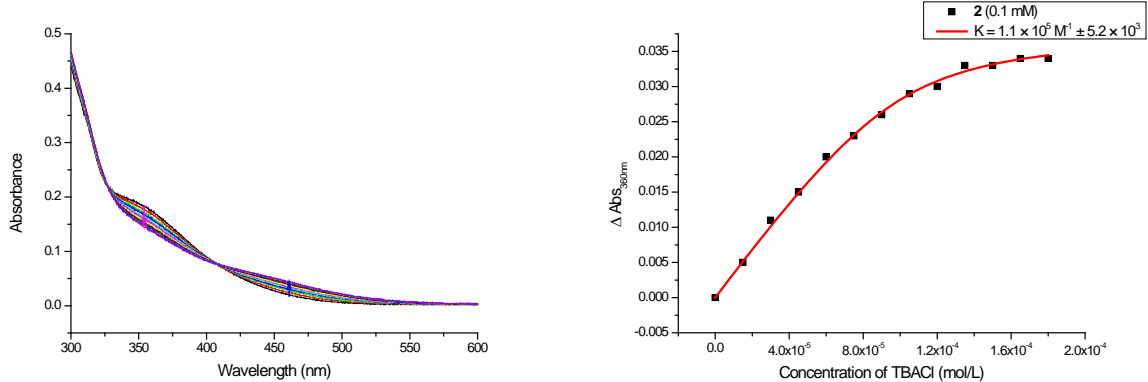


**Figure S21.** Changes in the electronic spectrum of DNP-C4P *trans*-**2** (acetonitrile solution; ambient temperature) seen upon the progressive addition of TBACl (left) and the corresponding binding isotherm analysis (right).

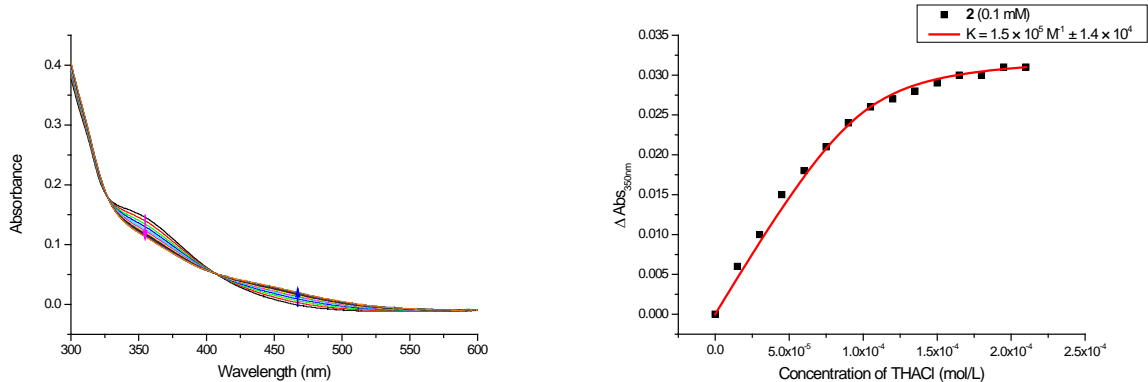


**Figure S22.** Changes in the electronic spectrum of DNP-C4P *trans*-**2** (acetonitrile solution; ambient temperature) seen upon the progressive addition of THACl (left) and the corresponding binding isotherm analysis (right).

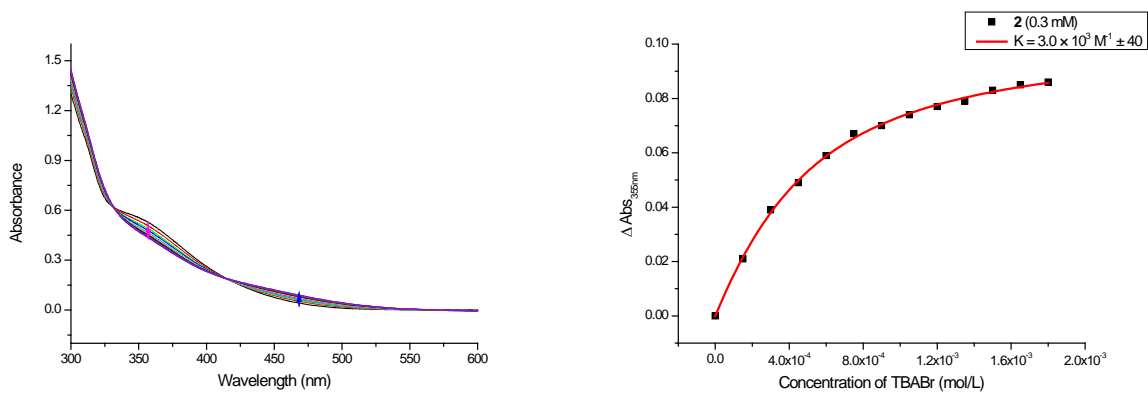


**Figure S23.** Changes in the electronic spectrum of DNP-C4P *trans*-2 (acetonitrile solution; ambient temperature) seen upon the progressive addition of TBABr (left) and the corresponding binding isotherm analysis (right).

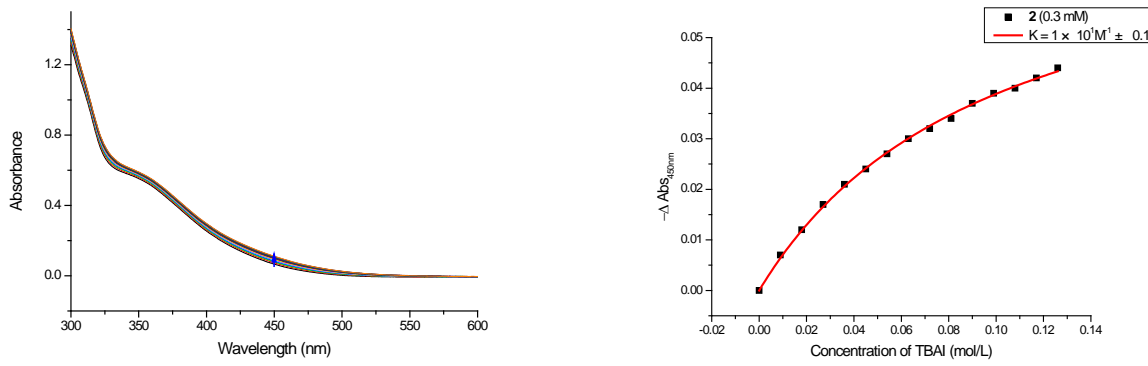


**Figure S24.** Changes in the electronic spectrum of DNP-C4P *trans*-2 (acetonitrile solution; ambient temperature) seen upon the progressive addition of TBAI (left) and the corresponding binding isotherm analysis (right).

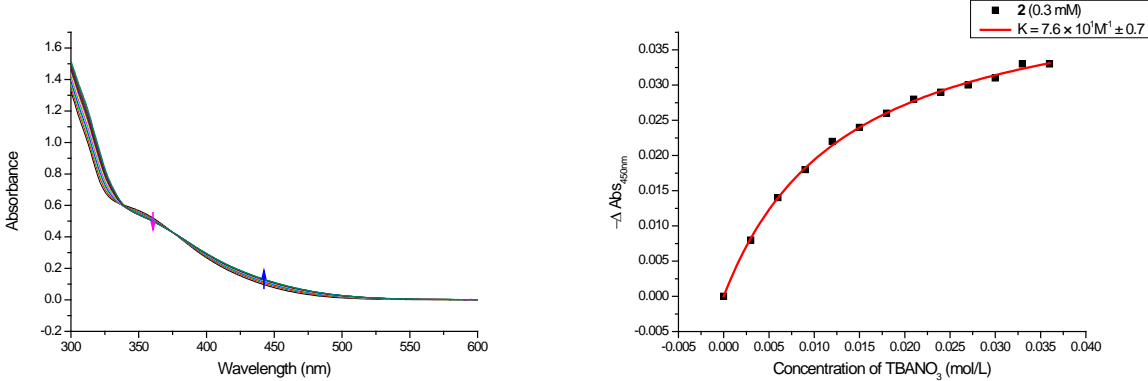


**Figure S25.** Changes in the electronic spectrum of DNP-C4P *trans*-2 (acetonitrile solution; ambient temperature) seen upon the progressive addition of TBANO<sub>3</sub> (left) and the corresponding binding isotherm analysis (right).

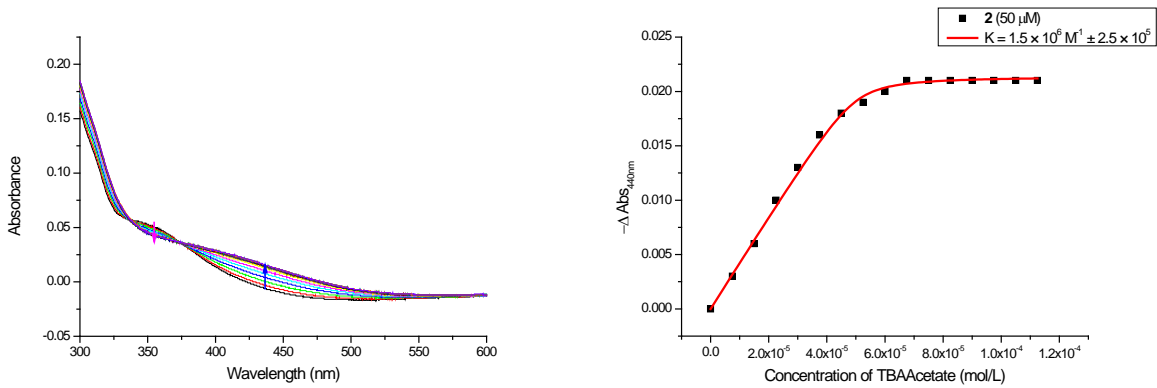


**Figure S26.** Changes in the electronic spectrum of DNP-C4P *trans*-2 (acetonitrile solution; ambient temperature) seen upon the progressive addition of TBAAcetate (left) and the corresponding binding isotherm analysis (right).

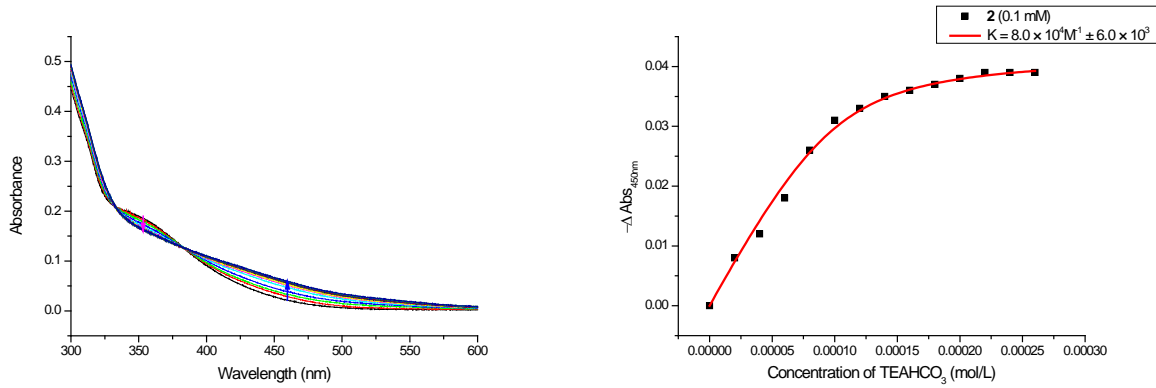


**Figure S27.** Changes in the electronic spectrum of DNP-C4P *trans*-2 (acetonitrile solution; ambient temperature) seen upon the progressive addition of TEAHCO<sub>3</sub> (left) and the corresponding binding isotherm analysis (right).

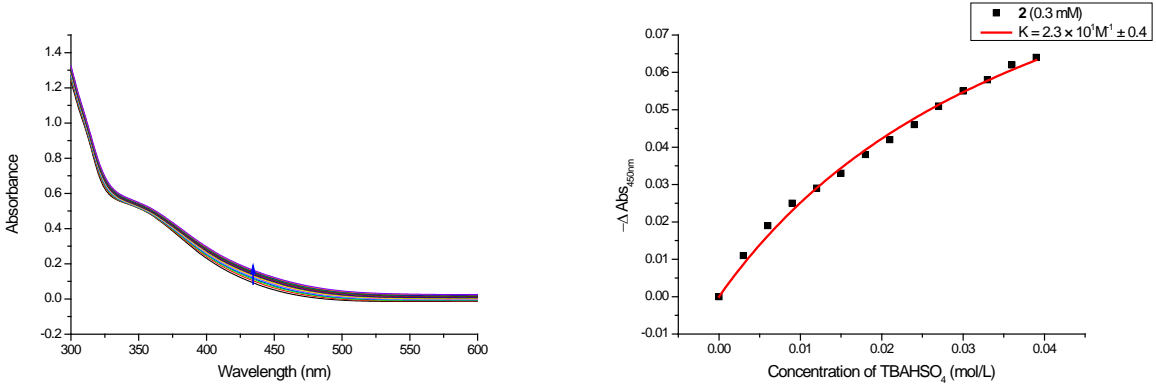


**Figure S28.** Changes in the electronic spectrum of DNP-C4P *trans*-2 (acetonitrile solution; ambient temperature) seen upon the progressive addition of TBAHSO<sub>4</sub> (left) and the corresponding binding isotherm analysis (right).

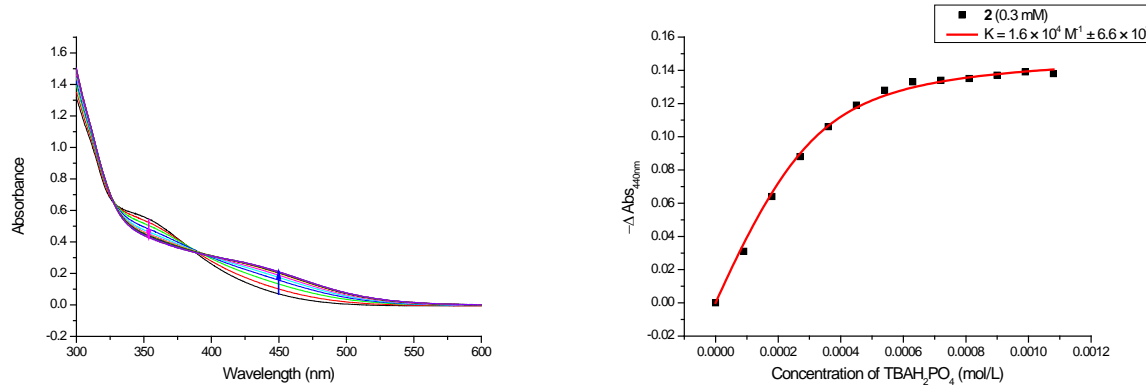


**Figure S29.** Changes in the electronic spectrum of DNP-C4P *trans*-2 (acetonitrile solution; ambient temperature) seen upon the progressive addition of TBAH<sub>2</sub>PO<sub>4</sub> (left) and the corresponding binding isotherm analysis (right).

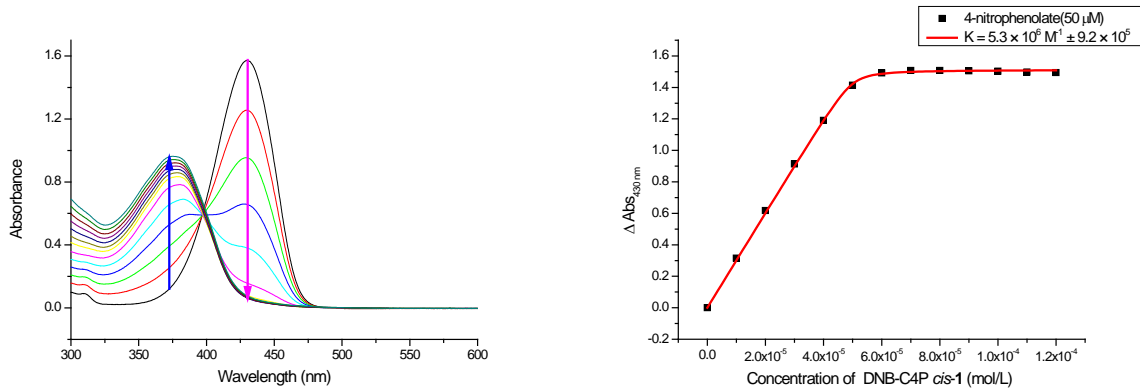


**Figure S30.** Changes in the electronic spectrum of 4-nitrophenolate (acetonitrile solution; ambient temperature) seen upon the progressive addition of DNP-C4P *cis*-1 (left) and the corresponding binding isotherm analysis (right).

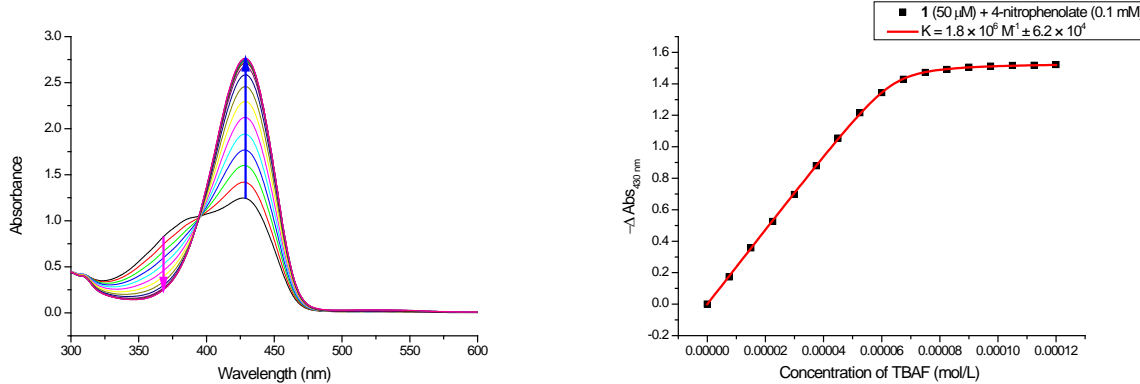


**Figure S31.** Changes in the electronic spectrum of a mixture of **1** (50  $\mu$ M) + 4-nitrophenolate (0.1 mM) (acetonitrile solution; ambient temperature) seen upon the progressive addition of fluoride anion (left) and the corresponding binding isotherm analysis (right).

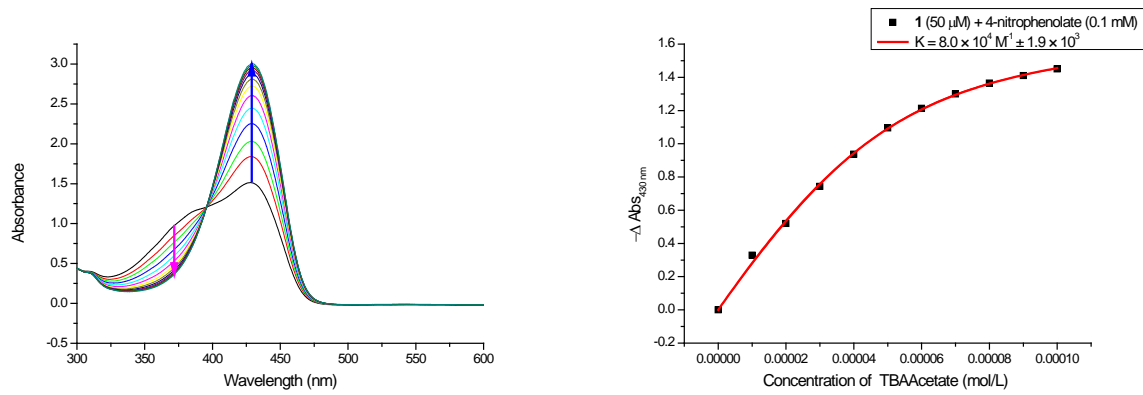


**Figure S32.** Changes in the electronic spectrum of a mixture of **1** (50  $\mu\text{M}$ ) + 4-nitrophenolate (0.1 mM) (acetonitrile solution; ambient temperature) seen upon the progressive addition of acetate anion (left) and the corresponding binding isotherm analysis (right).

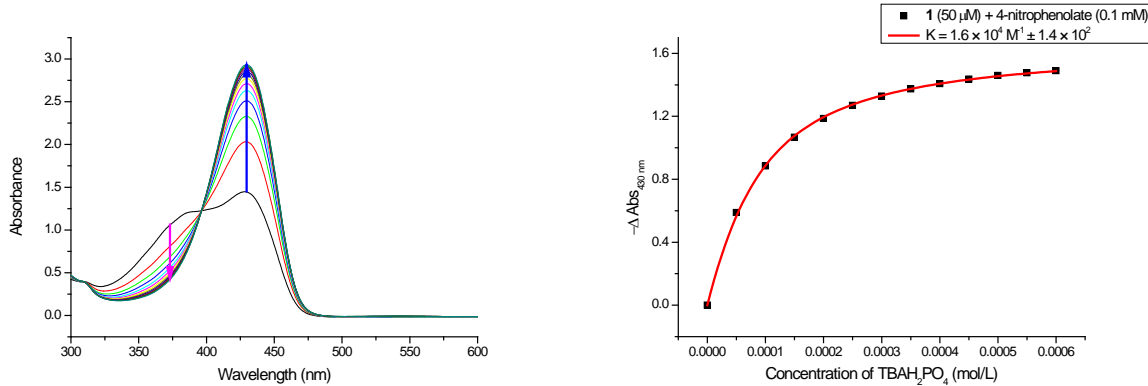


**Figure S33.** Changes in the electronic spectrum of a mixture of **1** (50  $\mu\text{M}$ ) + 4-nitrophenolate (0.1 mM) (acetonitrile solution; ambient temperature) seen upon the progressive addition of dihydrogen phosphate anion (left) and the corresponding binding isotherm analysis (right).

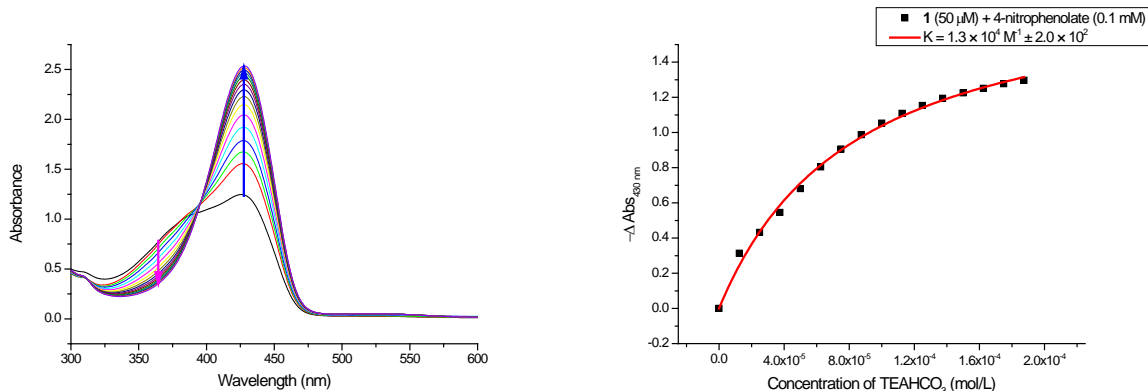


**Figure S34.** Changes in the electronic spectrum of a mixture of **1** (50  $\mu\text{M}$ ) + 4-nitrophenolate (0.1 mM) (acetonitrile solution; ambient temperature) seen upon the progressive addition of hydrogen carbonate anion (left) and the corresponding binding isotherm analysis (right).

**I-3.  $^1\text{H}$  NMR studies.**

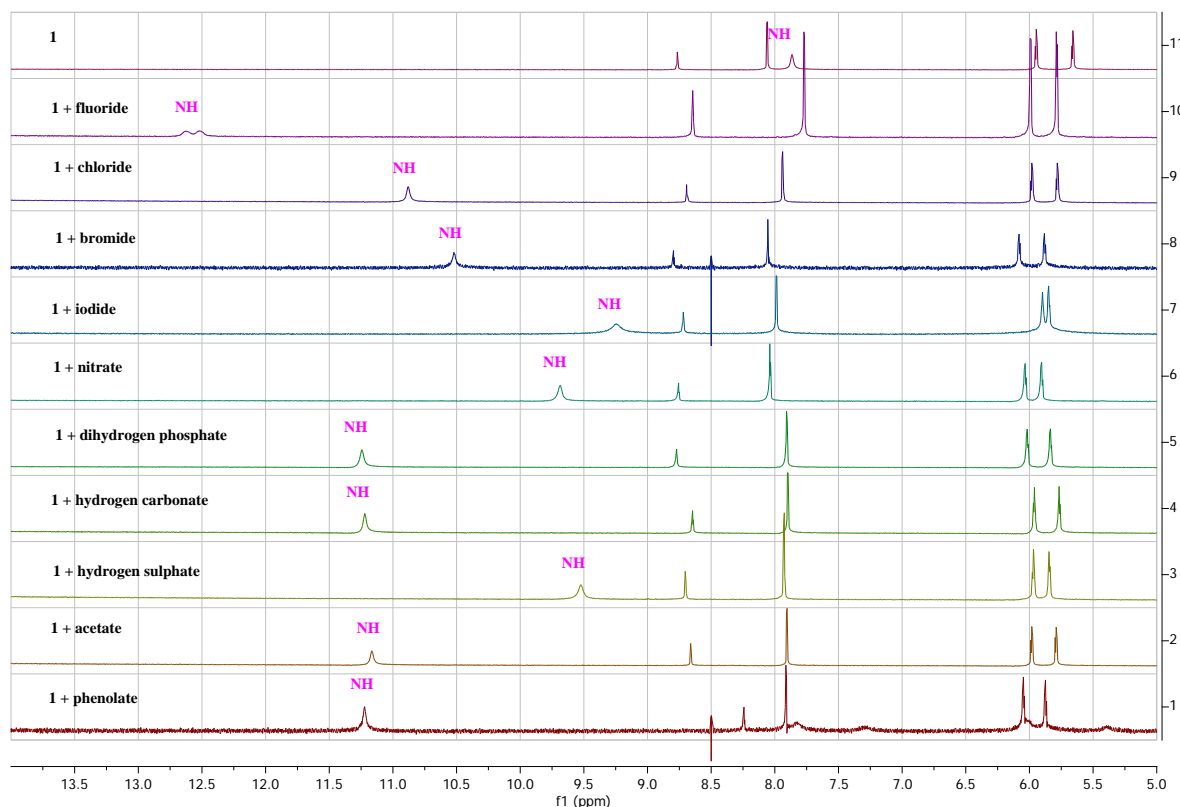


**Figure S35.**  $^1\text{H}$  NMR spectra of DNP-C4P *cis*-**1** with diverse anions (2 equiv.).

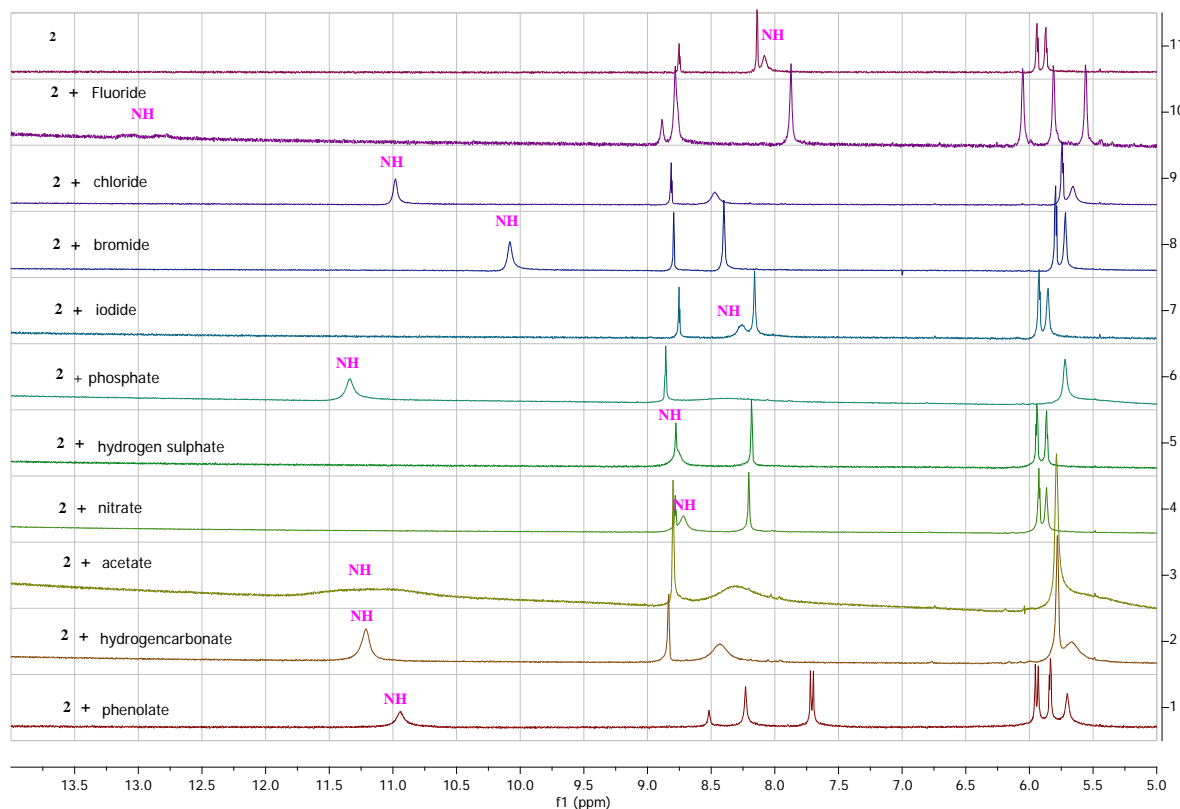


**Figure S36.**  $^1\text{H}$  NMR spectra of DNP-C4P *trans*-**2** with diverse anions (2 equiv.).

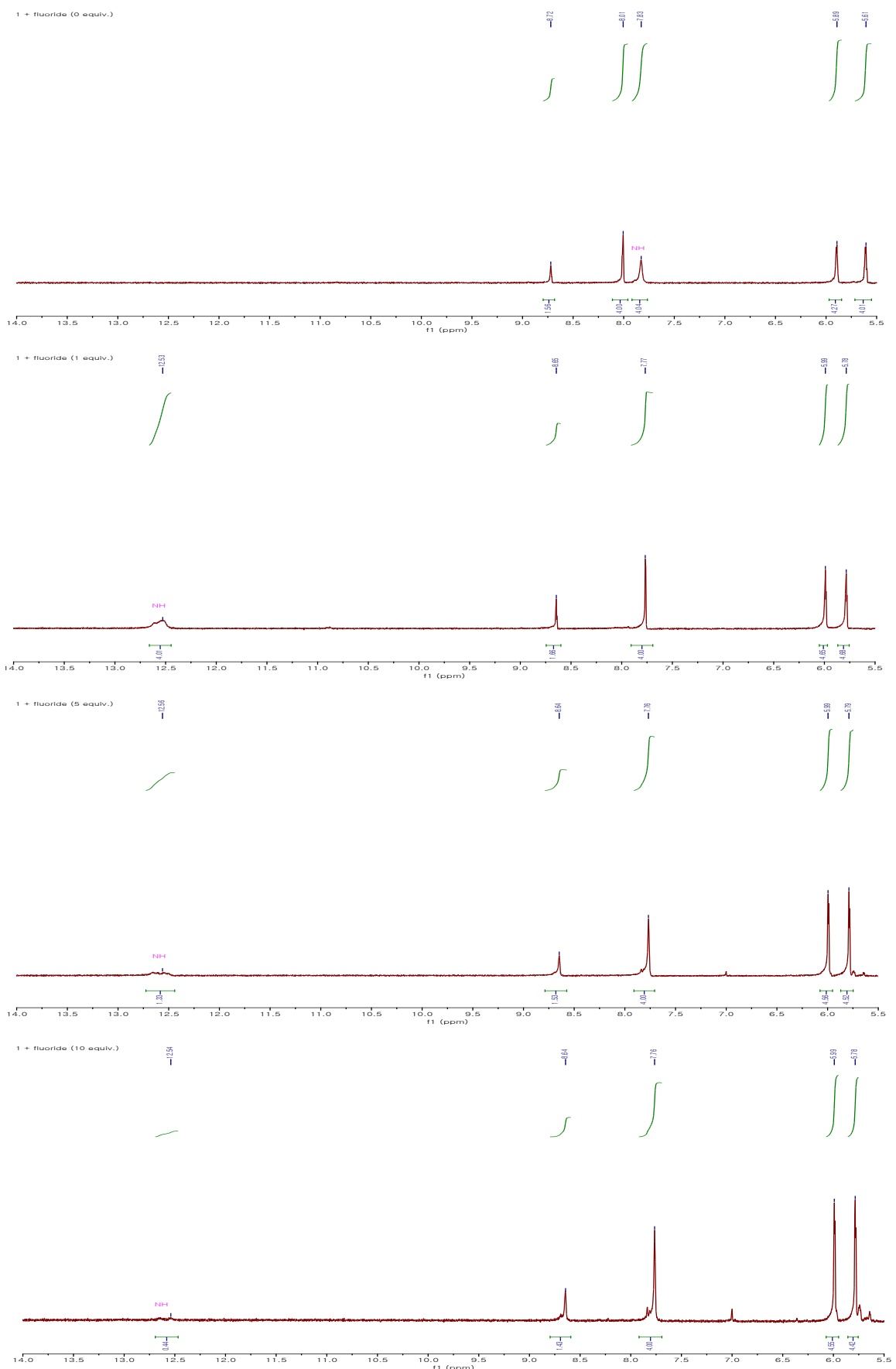


**Figure S37.**  $^1\text{H}$  NMR spectra of DNP-C4P *cis*-**1**(2 mM) with TBAF.

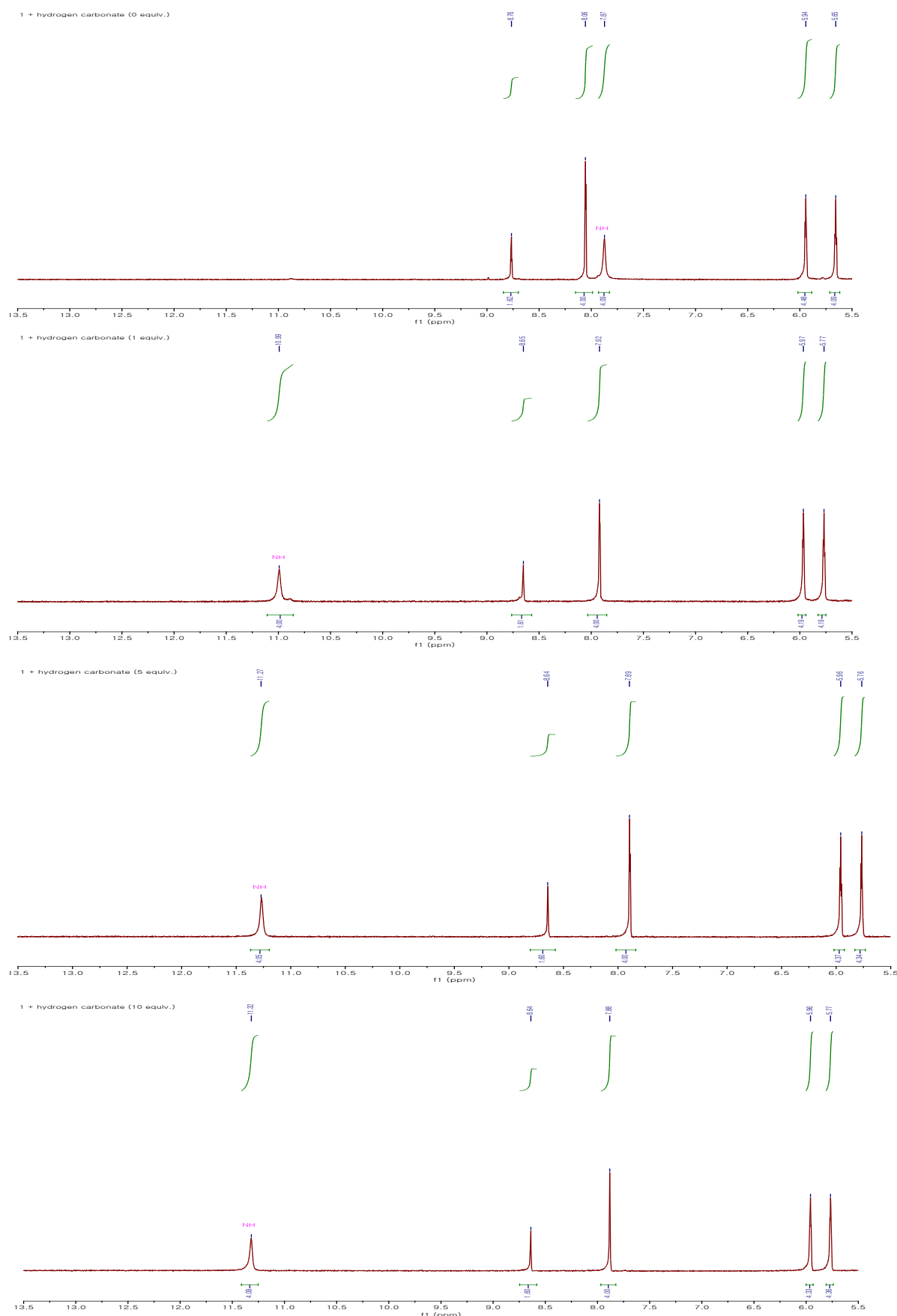
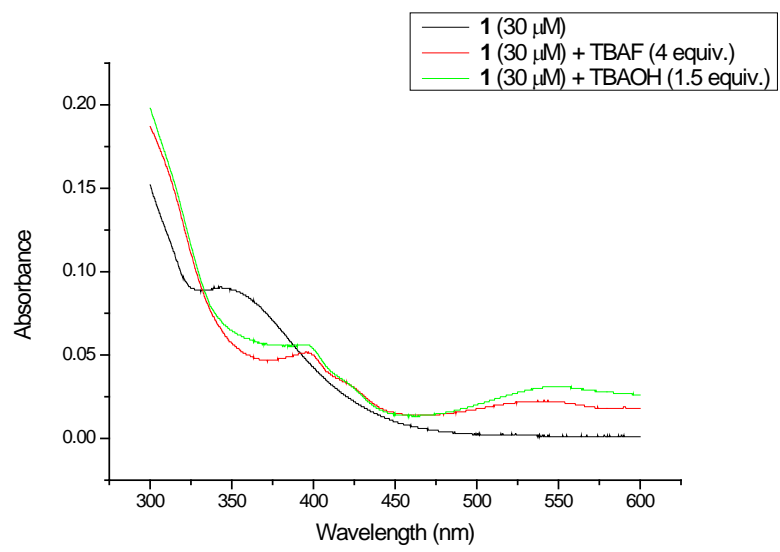


Figure S38. <sup>1</sup>H NMR spectra of DNP-C4P *cis*-1(2 mM) with TEAHCO<sub>3</sub>.



**Figure S39.** Comparison of UV-spectra of DNP-C4P *cis*-**1**(30  $\mu$ M) after addition of TBAF and TBAOH.